Solution Structure of Reduced Monomeric Q133M2 Copper, Zinc Superoxide Dismutase (SOD). Why Is SOD a Dimeric Enzyme?[†,‡]

Lucia Banci, Marco Benedetto, Ivano Bertini,* Rebecca Del Conte, Mario Piccioli, and Maria Silvia Viezzoli

Department of Chemistry, University of Florence, Florence, Italy

Received February 12, 1998; Revised Manuscript Received June 8, 1998

ABSTRACT: Copper, zinc superoxide dismutase is a dimeric enzyme, and it has been shown that no cooperativity between the two subunits of the dimer is operative. The substitution of two hydrophobic residues, Phe 50 and Gly 51, with two Glu's at the interface region has disrupted the quaternary structure of the protein, thus producing a soluble monomeric form. However, this monomeric form was found to have an activity lower than that of the native dimeric species (10%). To answer the fundamental question of the role of the quaternary structure in the catalytic process of superoxide dismutase, we have determined the solution structure of the reduced monomeric mutant through NMR spectroscopy. Another fundamental issue with respect to the enzymatic mechanism is the coordination of reduced copper, which is the active center. The three-dimensional solution structure of this 153-residue monomeric form of SOD (16 kDa) has been determined using distance and dihedral angle constraints obtained from ^{13}C, ^{15}N triple-resonance NMR experiments. The solution structure is represented by a family of 36 structures, with a backbone rmsd of 0.81 ± 0.13 Å over residues 3−150 and of 0.56 ± 0.08 Å over residues 3−49 and 70−150. This structure has been compared with the available X-ray structures of reduced SODs as well as with the oxidized form of human and bovine isoenzymes. The structure contains the classical eight-stranded Greek key β-barrel. In general, the backbone and the metal sites are not affected much by the monomerization, except in the region involved in the subunit−subunit interface in the dimeric protein, where a large disorder is present. Significative changes are observed in the conformation of the electrostatic loop, which forms one side of the active site channel and which is fundamental in determining the optimal electrostatic potential for driving the superoxide anions to the copper site which is the rate-limiting step of the enymatic reaction under nonsaturating conditions. In the present monomer, its conformation is less favorable for the diffusion of the substrate to the reaction site. The structure of the copper center is well-defined; copper(I) is coordinated to three histidines, at variance with copper(II) which is bound to four histidines. The hydrogen atom which binds the histidine nitrogen detached from copper(I) is structurally identified.

Superoxide dismutase (SOD) is a copper enzyme which has for many years attracted the interest of researchers, who have had different approaches and goals. In particular, it has been thoroughly characterized in terms of structure−function relationships so several aspects of the enzymatic reaction could be understood (*1*−*3*, and references therein). This enzyme is responsible of scavenging superoxide radicals, catalyzing their dismutation to molecular oxygen and hydrogen peroxide through the two-step reaction (*4*, *5*)

$$Cu^{2+} + O_2^- \rightarrow Cu^+ + O_2$$

$$Cu^+ + O_2^- + 2H^+ \rightarrow Cu^{2+} + H_2O_2$$

The observed rates for these reactions are very fast ($k_{obs} \cong 2-3 \times 10^9\ s^{-1}\ M^{-1}$) (*6*, *7*). The enzyme is active in both copper(II)- and copper(I)-containing forms. Under nonsaturating conditions, the rate-limiting step is the diffusion of substrate to the reaction site (*8*, *9*). The X-ray structure of the oxidized bovine isoenzyme has been known for more than 20 years (*10*), while more recently, those of the oxidized human isoenzyme (*11*) and of other isoenzymes (*12*−*18*) were reported. X-ray data are also available for the reduced species (*19*, *20*) which show some conflicting results (see later).

The protein is constituted by two identical subunits, which experience extensive contacts, mainly hydrophobic even if some hydrophilic interactions further stabilize the dimer. The interacting parts include the N-terminal and the C-terminal β-strands and two loops involving residues 49−54 (loop IV) and 102−114 (loop VI).

Each subunit is formed by a β-barrel, made of eight antiparallel (*20*) β-strands, connected by seven turns and loops. Among the latter, three loops (loops IV, VI, and VII) are long and have nonorganized secondary structure. The active site of each monomer contains one copper ion and one zinc ion. They are located between loops IV and VII,

[†] This work was financially supported by CNR, Commitato Nazionale Scienze Chimiche (Contract 96.00802.CT03), and was carried out under the TMR Large Scale Facility Program (PARABIO, ERBFMGECT950033).

[‡] The coordinates for the structure have been deposited in the Brookhaven Protein Data Bank under file name 1BA9.

* To whom correspondence should be addressed: Department of Chemistry, University of Florence, Via Gino Capponi, 7, I-50121 Florence, Italy. Fax: +39-55-2757555. Phone: +39-55-2757549. E-mail: bertini@lrm.fi.cnr.it.

S0006-2960(98)00347-X CCC: $15.00
Published on Web 08/05/1998

outside the β-barrel. In the oxidized enzyme, copper(II) is coordinated by four His's (His 46, 48, 120, and 63), one of which (His 63) makes a bridge between copper and zinc. The zinc ion is bound to three His's (His 63, 71, and 80) and to an Asp residue, Asp 83, which belongs to the β-barrel. A complex network of hydrogen bonds determines the orientation of the metal ligands. A long bridge between copper and zinc is formed by Asp 124 which connects, through H-bonds, His 71 and His 46. The zinc ion is completely buried in the protein. The copper ion sits at the bottom of the active site channel, a crevice 13 Å deep and 22 Å large, which narrows to 3 Å in the proximity of copper (*21*). The copper ion is solvent-exposed; a water molecule is positioned about 2.5 Å (Cu−O) from copper (*22*−*24*). A recent XAFS study places this water molecule at 2.2 Å at 77 K (*25*). Furthermore, a chain of well-ordered water molecules links this water molecule to the bulk solvent. The edge of the active site channel is constituted by charged residues, whose side chains form a H-bond network. These charged residues produce a positive electrostatic field which drives the negative superoxide ion toward the copper ion. The residues involved are Glu 132, Glu 133, Lys 136, and Thr 137 on one side of the channel and Arg 143 on the other side. The rim of the channel is completed by the side chains of Glu 120 and Lys 121.

A series of mutants have been produced and characterized on the residues of the active site channel (*26*−*37*). The functional characterization of the wild type enzyme and of the mutants and the dependence of the enzymatic activity on ionic strength have shown that electrostatic interactions are extremely important for determining the fast catalytic rates experienced by the enzyme, by increasing the diffusion of the substrate in the channel toward copper. Activity measurements have also shown that there is no cooperativity between the two subunits of the dimer (*38*).

The disruption of the quaternary structure of SOD can be created by mutation of some residues in the interface region. Indeed, substitution of two hydrophobic residues, Phe 50 and Gly 51, with two Glu's produced a soluble monomeric form (*39*).

However, this monomeric form had a much lower activity than the native dimeric species (*39*). This behavior raises the fundamental question about the role of the quaternary structure of superoxide dismutase in the biological function. Why has nature produced a dimer made by two identical subunits when they work independently? And why are they much less active when they are separated? To answer these questions and to further understand the structure−function relationship of SOD, we have undertaken the determination of the solution structure through NMR spectroscopy of one of the available monomers. The relatively low molecular weight of the monomer species (16 000) and the possibility of totally labeling the protein with ^{13}C and ^{15}N make the determination of the solution structure a feasible goal. X-ray structures of both oxidized and reduced dimeric species are available for the yeast and for the bovine isoenzymes (*10*, *14*, *19*, *20*). In the reduced form, the bridge between copper and zinc is broken at the Cu−Nϵ2 bond, and in the oxidized form, the bridge is intact. On the other hand, it has been definitively shown by NMR that in solution the bridge is broken in the reduced dimeric protein (*40*, *41*). The structure determination in solution is also aimed at definitively describing the species in a medium close to the physiological one. Indeed, NMR spectroscopy can clearly monitor the protons and therefore can unequivocally describe the protonation status of the His which is bridging in the oxidized form.

We report here the three-dimensional solution structure of the reduced monomeric form obtained by conversion of the two hydrophobic residues, Phe 50 and Gly 51, to two negative hydrophilic Glu groups (hereafter M2SOD). In this system, Glu 133 has also been changed to a neutral group (Gln) (hereafter Q133M2SOD). It has been shown that substitution of this residue with the neutral Gln increases 2−3-fold the catalytic activity of both the dimeric protein (*31*) and the monomeric protein (*42*).

The NMR structure is compared with the available X-ray structures of reduced SODs as well as with the oxidized forms of human and bovine isoenzymes.

MATERIALS AND METHODS

Sample Preparation. The monomeric species of human SOD, where the Phe 50 and Gly 51 residues at the subunit−subunit interface have been replaced by two hydrophilic Glu residues and where a further mutation at position 133 (Glu to Gln) has been introduced (Q133M2SOD), has been expressed as previously reported (*42*). The *Escherichia coli* TOPP1 strain (Stratagene) was transformed with the plasmid carrying the mutated SOD gene. The cells were grown in ^{13}C- and ^{15}N-enriched M9 minimal medium, as previously described (*43*). The protein was isolated and purified as previously reported (*31*). The resulting samples were fully enriched in ^{15}N and ^{13}C. The copper and zinc content was checked through atomic absorption analysis with a GBC 903 instrument. Reduction was achieved by addition of a 0.1 M solution of sodium isoascorbate (the final concentration of isoascorbate was in the range of 4−6 mM, i.e., twice the copper concentration) in phosphate buffer, under anaerobic conditions, at pH 5.0. The H_2O sample contained 10% D_2O for the lock signal.

The presence of a cystine bridge was observed with a SDS−acrylamide gel. The protein was treated with dithiothreitol (DTT) as a reducing agent and compared to a nontreated sample. The dimeric wild type (WT) was also used as a control experiment.

NMR Spectroscopy. The NMR experiments were recorded on Bruker AMX 600 and Avance 800 spectrometers, operating at 14.1 and 18.7 T, respectively. All experiments were performed with a triple-resonance 5 mm probe and with a BGU unit for self-shielded z-gradients. All NMR experiments were carried out at 298 K, unless otherwise specified.

To identify side chain spin patterns, an (H)C(CO)NH-TOCSY (*44*) experiment was recorded in H_2O solution, together with (H)CCH-TOCSY and H(C)CH-TOCSY experiments (*45*) carried out in D_2O solutions.

NOESY−^{15}N HSQC and NOESY−^{13}C HSQC experiments (*46*) were performed to obtain dipolar connectivities, and a HNHA experiment was performed to extract ^3J HNHA coupling constants (*47*) which are used in structure calculations. All the experiments were performed using pulsed field gradients (PFG) along the *z* axis. For most of the experiments, PFG were applied during INEPT and inverse INEPT transfers. Unless otherwise indicated, quadrature detection

in the indirect dimensions was performed in the TPPI mode (*48*), and water suppression was achieved with a Watergate sequence (*49*).

For the assignment of side chains, (H)CCH-TOCSY and H(C)CH-TOCSY experiments were performed at 600 MHz, using 512 (^{1}H) × 74 (^{13}C) × 74 (^{13}C) and 512 (^{1}H) × 74 (^{13}C) × 174 (^{1}H) points, respectively. Spectral windows of 5000 Hz (^{1}H) × 9615 Hz (^{13}C) × 9615 Hz (^{13}C) and of 5000 Hz (^{1}H) × 9615 Hz (^{13}C) × 4000 Hz (^{1}H), respectively, were used. Both experiments were performed using PFG for coherence selection and States (*50*) and echo−antiecho modes for indirect dimensions. The (H)C(CO)NH-TOCSY experiment was carried out with 2048 (^{1}H) × 64 (^{15}N) × 192 (^{13}C) data points over spectral windows of 10 535 Hz (^{13}C) × 1712 Hz (^{15}N) × 7788 Hz (^{1}H). To identify the coordination mode of metal binding histidines, a ^{15}N HSQC experiment was performed for measuring $^2J_{N\epsilon H\delta}$, $^2J_{N\epsilon H\epsilon}$, $^2J_{N\delta H\epsilon}$, and $^3J_{N\delta H\delta}$ coupling constants (*51*). In this experiment, the INEPT delay was set to 22 ms.

Experiments for obtaining constraints for structure calculations, i.e., ^3J coupling constants and NOE intensities, were carried out at 800 MHz. To extract $^3J_{HNH\alpha}$ coupling constants, a HNHA experiment was carried out using 2048 real (^{1}H), 46 complex (^{15}N), and 56 complex (^{1}H) data points. States−TPPI was used for both indirect dimensions. The final data matrix was constituted by 512 (^{1}H) × 128 (^{1}H) × 512 (^{15}N) data points. NOESY−^{15}N HSQC spectra were recorded with 2048 (^{1}H) × 96 (^{15}N) × 340 (^{1}H) data points. Spectral windows of 3012 and 9615 Hz were used, respectively, for ^{15}N and both ^{1}H dimensions. The mixing time was 130 ms. NOESY−^{13}C HSQC spectra were collected with 2048 (^{1}H) × 256 (^{1}H) × 128 (^{13}C) data points. Spectral windows of 19 230 and 9615 Hz were used, respectively, for ^{13}C and both ^{1}H dimensions. The mixing time was 100 ms. Watergate 2D NOESY experiments were carried out to identify connectivities involving histidines of the active site. Data for an 8K × 2K data point matrix were collected at 298 K using a mixing time of 130 ms. A similar experiment was carried out at 288 K, with a mixing time of 60 ms over a 2K × 1K data point matrix.

Data were processed with the standard Bruker software packages (UXNMR and XWINNMR) or with the software package PROSA (ETH, Zurich, Switzerland) (*52*). Data analysis and assignment were performed using the program XEASY (ETH) (*53*).

Structure Calculations and Refinement. Intensities of dipolar connectivities in three-dimensional ^{15}N- or ^{13}C-edited NOESY and in two-dimensional NOESY spectra, obtained using a 130 or 60 ms mixing time, were measured using the integration routines present in the program XEASY (*53*). The majority of cross-peaks have been obtained from the 3D NOESY−^{15}N HSQC experiment. For those regions of the spectrum in which there is enough resolution to evaluate cross-peak intensities from homonuclear experiments, 2D NOESY was used. Dipolar connectivities involving Hα protons have been detected in the NOESY−^{13}C HSQC experiment. Peak volumes were converted into upper limits of interatomic distances by following the methodology of the program CALIBA (*54*). All the NOE cross-peaks were divided in different classes according to the nature of the protons involved, and each class was calibrated independently. Cross-peaks corresponding to fixed distances were initially used for the calibration. Calibration was then modified iteratively during the structure calculation process. As far as the cross-peaks involving protons of the metal ligand histidines are concerned, due to the fractional intensity of the imidazole HN signals of these residues, an independent calibration was used for each histidine. The intensities of intraring connectivities of each histidine were used as calibration factors to convert peak volumes into upper distance limits for those cross-peaks arising from the same histidine. $^3J_{HNH\alpha}$ coupling constants were obtained from the ratio between the intensity of the diagonal peak and that of the cross-peak integrated on the ^{1}H−^{1}H slices of the HNHA experiment where the cross-peak has the maximum intensity. The scalar coupling constants were converted into dihedral angle constraints by means of the appropriate Karplus relationship (*53*). The parameters used for each type of ^3J coupling constants were those previously published (*47*, *55*−*57*). For $^3J_{HNH\alpha}$ values of >8 and <4.5 Hz, the ϕ angle was assumed to be between −155 and −85° and between −70 and −30°, respectively.

The three-dimensional structure was calculated with the program DYANA (*58*). Four hundred random structures were annealed in 18 000 steps using the NOESY and angle constraints. Stereospecific assignments were obtained with the program GLOMSA (*54*).

Metal ions were added in the DYANA calculations using a special linker (pseudoresidue) called LTNS. A linker is a rigid sequence of six dummy atoms spaced 1 Å from one another, making 90° angles and allowing free rotation about the central bond between atoms 3 and 4. Linkers can be chained as many times as needed by overlapping the last three atoms of one linker with the first three atoms of the next, in such a way to cover 1 Å each. The chain of linkers does not affect the minimization algorithm as the dummy atoms have null van der Waals radii. The last dummy atom in the chain of linkers represents the metal ion (ME) to which a van der Waals radius of 1.64 Å has been assigned. To allow the two metal ions to span the whole space occupied by the macromolecule, the protein was extended with a long chain of 58 linkers in which one metal ion is placed after 29 linkers (covering a distance of 30 Å) and the second is placed at the end of the chain. Each metal ion is then linked to the imidazole nitrogen atoms of the coordinated His or to the Oδ1 of Asp 83, with the N-ME or O-ME distance ranging between a lower limit of 1.8 Å and an upper limit of 2.3 Å. The coordination site of each histidine (i.e., which histidines should be coordinated to which of the two metal ions) has been determined by perfoming a preliminary DYANA calculation without inserting the metal ions. This calculation defined the conformation of the ligands around the metal sites, and therefore their coordination mode. The interresidue NOEs unambiguously determine the histidine conformations in such a way that His 46, His 48, and His 120 are bound to one of the two metal ions, His 71, His 80, and Asp 83 are bound to the other, while His 63 could be bound to any of the two metal ions. The ^{1}H−^{15}N HSQC experiment tailored to measure the ^2J NH couplings allowed us to indentify, for each His, the nature of the N atom coordinating the metal ion. The linkers only define the metal−nitrogen distances, leaving the conformation of the histidines completely free. In other words, the bond angles at the copper and zinc ions are not imposed but can freely change in the structural

calculations, being determined only by the experimental inter-histidine NOEs.

The chemical shift value of the Cys 146 Cβ atom is indicative of the presence of a disulfide bridge between Cys 146 and the unassigned Cys 57 (*59*). The presence of such a bond has been confirmed by the experiment with SDS−polyacrylamide gel electrophoresis (see Sample Preparation). Therefore, the Sγ−Sγ distance for these residues was supposed to range between an upper limit of 2.1 Å and a lower limit of 2.0 Å.

The final DYANA family was formed by the 36 structures with the lowest target function.

Refinement was performed with restrained energy minimization with the Sander module of the program AMBER (*60*). The setup was the same as that used for restrained energy minimization and dynamics of the reduced form of the dimeric protein (*19*). In particular, the charges of the metal ions and their ligands were taken from that work and the other force field parameters were set like those previously reported (*19*, *61*). Force constants of 32 kJ mol^{-1} for the distance and the angular constraints were used (*62*). The restrained energy minimization calculations were performed, in vacuo, following the setup previously reported (*19*).

The quality of the obtained structures was checked using the program PROCHECK-NMR (*63*) and Ramachandran analysis. Structure calculations and analysis were performed on an IBM SP02 parallel computer.

RESULTS AND DISCUSSION

Assignment of Side Chains. The set of experiments used to perform the backbone assignment and to establish the elements of secondary structure of the present monomer (*43*) was also used to extend the assignment to most of the proton and carbon atoms of the side chains. In particular, H(C)-CH-TOCSY (*45*), (H)CCH-TOCSY (*45*), and (H)C(CO)NH-TOCSY (*44*) experiments provided most of the information used for the assignment of the side chain protons (first experiment) and of the side chain carbons (the other two experiments). The first two experiments, carried out with a sample in D_2O, turned out to be particularly useful for those residues whose HN signals were not observed or significantly broadened because of their exchange with the bulk solvent. The overall assignment of side chain protons and carbon resonances is reported as Supporting Information. Ninety-three percent of the side chain proton resonances have been assigned. Overall, 88% of the total proton resonances have been assigned. No information was obtained on the side chains of the two residues, Cys 57 and Thr 58, for which no backbone signal was previously assigned (*43*). The complete ^{1}H, ^{13}C, and ^{15}N resonance assignment is reported in the Supporting Information.

Assignment of Active Site Residues. Figure 1 shows a comparison of the 16−12 ppm region of the ^{1}H NMR spectrum obtained at pH 5.0 with different suppression schemes of the water signal (Figure 1A−C). At this pH value, all the metal-coordinated histidines are protonated at the ring nitrogen not involved in a bond with the metal ion. Consistent with what has previously been observed in the reduced form of the dimeric protein (*40*) and of the M2 monomeric analogue (*39*), the intensities of the histidine ring HN signals are strongly dependent on the solvent suppression

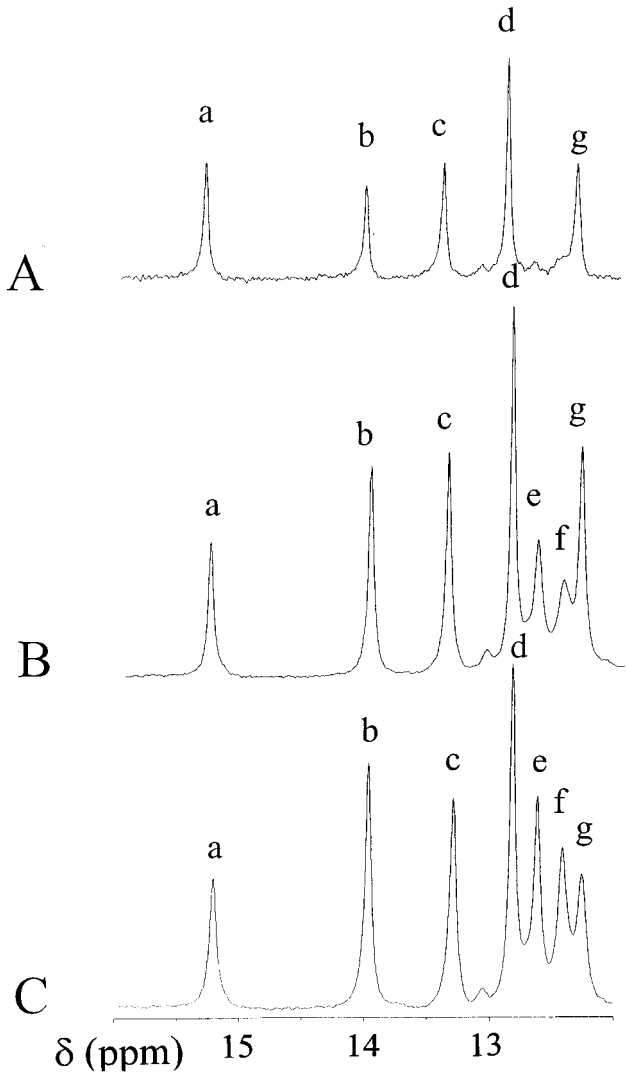

FIGURE 1: 800 MHz, ^{1}H NMR spectra of the 16−12 ppm region of the Q133M2SOD derivative in 20 mM phosphate buffer at pH 5.0 obtained with different suppression schemes of the water signal: (A) presaturation at 298 K, (B) Watergate suppression at 298 K, and (C) Watergate suppression at 288 K. Signal assignment was as follows: (a) HNϵ2 His 71, (b) HNϵ2 His 43, (c) HNϵ2 His 46, (d) HNδ1 His 43, (e) HNϵ2 His 80, (f) HNϵ2 His 63, and (g) HNδ1 His 48.

scheme as these protons exchange relatively fast with the bulk solvent. This could be related to their different solvent accessibilities. From their behavior, it appears that the solvent accessibility of His 80 and His 63 in this derivative is larger than that in the case of the reduced dimeric protein and of the monomeric M2SOD (*39*). In the latter derivatives, the imidazole HN signals of His 80 and His 63 can be easily detected at 298 K, with a 1331 (*64*) and a Watergate (*49*) pulse scheme for water suppression. On the other hand, in this derivative, the exchange with the bulk solvent results more quickly, as a 10 K decrease in temperature (288 K) is required to detect them.

The assignment of the ^{1}H signals of the ring protons of the coordinated histidines is obtained from the ^{1}H NOESY experiments. Their shifts are almost identical to those observed for the reduced M2SOD derivative (*39*). The ^{15}N resonances of the histidine rings can easily be individually defined in the ^{1}H−^{15}N HSQC experiment on the basis of their shift values. Furthermore, the resonances due to the

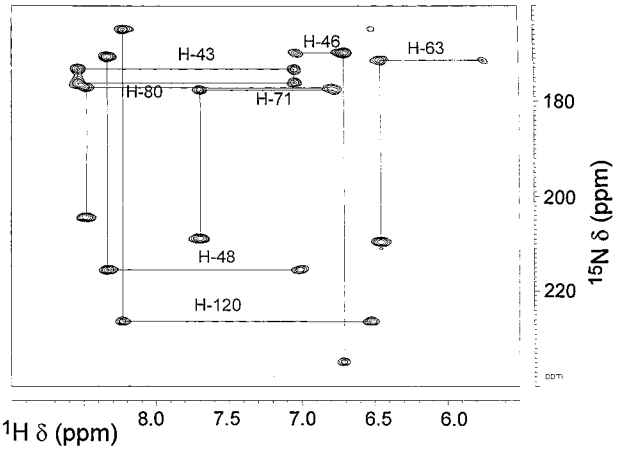

FIGURE 2: 800 MHz, ^{1}H−^{15}N HSQC spectrum of Q133M2SOD obtained using 22 ms for the INEPT transfer delay. The sample conditions are as described in the legend of Figure 1.

nitrogens coordinated to the metal ions have shift values around 220 ppm while the noncoordinated nitrogens have values of around 180 ppm (*51*). The assignment of each ^{15}N resonance to the specific nitrogen type (i.e., Nδ1 or Nϵ2) can be determined through ^{1}H−^{15}N heteronuclear experiments, by detecting the ^{2}J ^{15}N−^{1}H coupling between the imidazole nitrogen and the nonexchangeable imidazole protons (*65*−*67*). Figure 2 shows a portion of the ^{1}H−^{15}N HSQC spectrum collected using the INEPT delay optimized for detecting ^{2}J ^{15}N−^{1}H couplings. Nϵ2 nuclei experience two ^{2}J couplings, i.e., with Hϵ1 and Hδ2, while the Nδ1 nuclei experience only one ^{2}J coupling with Hϵ1. Through the sequence-specific assignment of proton resonances, the sequence-specific assignment of ^{15}N resonances is also obtained. It turns out that His 48 and His 120 are coordinated to the metal ion through the Nϵ2 atom and that His 46, 63, 71, and 80 are coordinated through the Nδ1 atom. In addition, this experiment shows that the imidazolate bridge between the two metal ions, formed by His 63 in the oxidized form, is broken at the Cu−Nϵ2 bond, while the Zn−Nδ1 bond of His 63 is conserved.

Structure Calculations. A total of 2508 upper distance limits and 65 dihedral angle constraints were assigned. They were used as input for the program DYANA (*58*). Of these constraints, 469 upper distance limits were found to be irrelevant as they can never be violated or arise from protons at fixed distances. A total of 2039 upper distance limits and 65 angle constraints together with 16 hydrogen bonds were used in all the subsequent calculations. Criteria for the identification and use of H-bonds have been previously reported (*68*). The number of costraints, divided in classes, are listed in Table 1. The average number of meaningful structural constraints per residue is 13.8. The number of experimental NOEs per residue (subdivided according to their class) is reported in Figure 3A. Twenty-nine stereospecific assignments were obtained with the program GLOMSA (*54*). The metal ions have been included by allowing copper to bind to Nϵ2 of His 48 and His120 and to Nδ1of His46 and allowing zinc to bind to Nδ1of His 63, 71, and 80 and to Oδ1 of Asp 83. Lower and upper distance limits of 1.8 and 2.3 Å, respectively, were imposed between the metal ions and the donor atoms (see Materials and Methods for the strategy of the procedure).

A family of 36 structures with a target function lower than 2.0 Å^2 (the best structure has a target function of 1.21 Å^2) was obtained. These values correspond to an rmsd for the experimental constraint of 0.026 ± 0.08 Å. This family of structures was refined by performing restrained energy minimization on each member. The final family is characterized by an average rmsd value from the mean structure of 0.81 ± 0.13 Å for the backbone atoms and of 1.23 ± 0.14 Å for the heavy atoms (the rmsd values are calculated

Table 1: Restraint Violations and Structural and Energetic Statistics for the Solution Structure of Reduced Q133M2SOD[a]

	REM	⟨REM⟩
rms violations per experimental distance constraint (Å)[b]		
intraresidue (309)	0.025 ± 0.003	0.023
sequential (589)	0.015 ± 0.002	0.013
interresidue short-range ($1 < \|i-j\| \leq 5$) (253)	0.024 ± 0.005	0.030
interresidue long-range ($\|i-j\| > 5$) (888)	0.024 ± 0.002	0.022
total (2039)	0.022 ± 0.001	0.021
rms violations per experimental dihedral angle constraint (deg)[b] (65)	1.85 ± 0.31	1.81
average number of violations per structure		
intraresidue	13.39 ± 2.23	12
sequential	14.08 ± 2.68	13
interresidue short-range ($1 < \|i-j\| \leq 5$)	14.17 ± 2.64	16
interresidue long-range ($\|i-j\| > 5$)	43.11 ± 4.07	34
dihedral angle	6.78 ± 1.97	6
total	84.75 ± 6.26	75
violations larger than 0.3 Å	0.22 ± 0.41	0
violations between 0.1 and 0.3 Å	31.47 ± 4.58	34
largest violation (Å)	0.38	0.28
energy of nonbonded interactions (kJ mol^{-1})	−9816 ± 297	−10140
PROCHECK-NMR[c]		
% of residues in most favored regions	67.60 ± 2.44	73.0
no. of bad contacts/100 residues	0.058 ± 0.20	0
H-bond energy (kJ mol^{-1})	3.18 ± 0.15	3.13
overall *G*-factor	−0.39 ± 0.02	−0.41

[a] REM indicates the energy-minimized family of 36 structures, and ⟨REM⟩ is the energy-minimized average structure obtained from the coordinates of the individual REM structures, best fitted to each other. [b] The number of experimental constraints for each class is reported in parentheses. [c] The program PROCHECK-NMR (*63*) was used to assess the overall quality of the structure. For the PROCHECK statistic, less than 10 bad contacts per 100 residues, an average hydrogen bond energy in the range of 2.5−4.0 kJ mol^{-1}, and an overall *G*-factor larger than −0.5 are expected for a good quality structure.

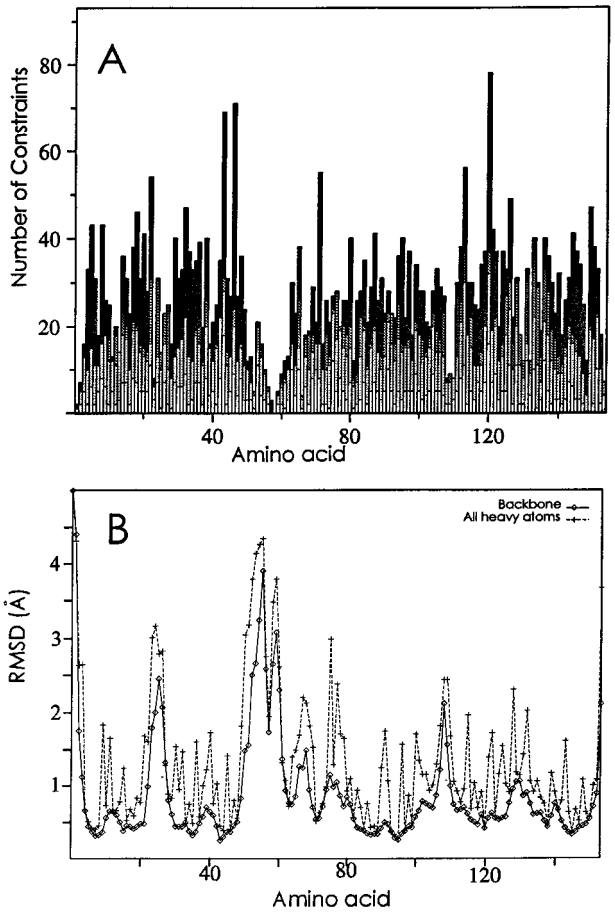

FIGURE 3: (A) Number of intraresidue (white), sequential (light gray), medium-range (gray), and long-range (black) NOEs per residue in reduced Q133M2SOD. (B) Backbone (◇) and heavy atom (+) rmsd values per residue with respect to the average structure of Q133M2SOD.

for residues 3−150). The rmsd per experimental constraint is 0.019 ± 0.006 Å. The rmsd values per residue, with respect to the average structure, are shown in Figure 3B. The structures of the family have been averaged and then minimized to produce the average structure used in the following analysis. A statistical analysis of the family of structures and of the average structure is reported in Table 1. It can be seen that the agreement with the experimental constraints is quite good, for all their types, with very low violation constraints within each class.

General Shape of the Protein and Comparison with X-ray Data. A tube representation of the family of structures (backbone and metal ions only) is shown in Figure 4. The quality of the structure was assessed through back-calculation of the NOESY cross-peaks on the minimized averaged structure. The calculation, carried out with the CORMA program (*69*, *70*) by using a single correlation time, was performed for the NOESY−^{15}N HSQC spectrum as the large majority of the peaks were assigned in this map. This analysis showed that a very small number of expected NOEs with significant intensity, located in disordered regions, are missing in the experimental maps and that all the expected NOEs between assigned protons have been assigned. The structure was evaluated with the Ramachandran plot and the PROCHECK-NMR analysis (Table 1). It turns out that 96% (117 residues) of the non-glycine and non-proline residues have the φ angle in the allowed region, 1.6% (two residues)

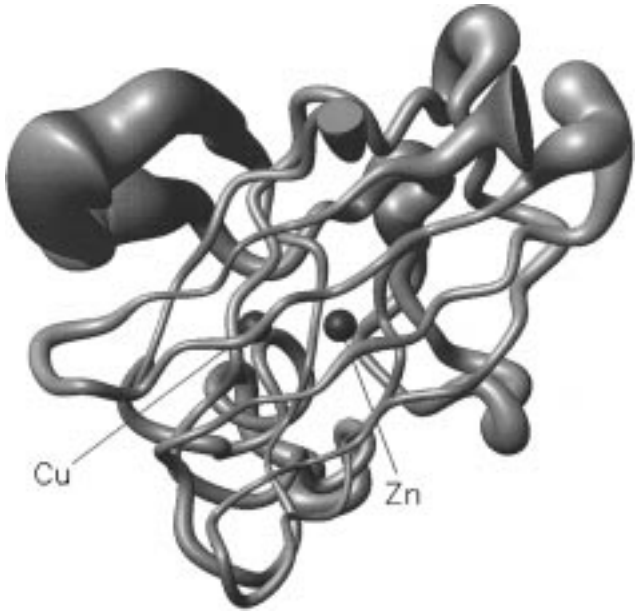

FIGURE 4: Tube representation of the family of 36 accepted structures of Q133M2SOD obtained with DYANA calculations and refined with REM calculations. Structures were aligned by best-fit superimposition of C, Cα, and N atoms of residues 3−48 and 63−150. The drawing was produced with MOLMOL (*78*).

in the generously allowed regions, and 2.5% (three residues) in the disallowed regions. The three residues in the disallowed regions are Lys 23, Glu 50, and Ala 55 which belong to regions of high disorder. Also, the two residues that are in the so-called "generously allowed regions" (Thr 54 and Ala 60) belong to disordered loop IV.

The PROCHECK-NMR analysis identified the following secondary structure elements: eight β-strands made up of residues 3−9, 15−21, 29−36, 41−48, 83−89, 96−101, 116−120, and 143−151 and an α-helix for residues 132−137. The structure shows the typical SOD Greek key, formed by an eight-stranded β-barrel. Such secondary structure, which was previously predicted from the analysis of medium- and long-range backbone NOEs (*43*), is very well-defined. The average rmsds for the protein segments of the β-barrel are 0.30 ± 0.05 and 0.80 ± 0.08 Å for backbone and all heavy atoms, respectively. This shows that the β-strands are characterized by lower disorder than the loops connecting them. Other than the N- and C-terminal parts, the most disordered regions are those extending from residue 23 to 27 (belonging to loop II) and from residue 50 to 68 (belonging to loop IV). A disorder larger than the average rmsd (see Figure 3B) is present also for residues 107−110 (belonging to loop VI).

The high rmsd values for the residue stretch of 50−69 are particularly striking, possibly an indication of local mobility (study in progress). The global average rmsd values for backbone and all heavy atoms drop to values of 0.56 ± 0.08 and 1.04 ± 0.08 Å, respectively, when they were calculated without residues 50−69. This protein stretch, which contains the two mutated residues (Phe 50 and Gly 51) in the present monomeric species, is involved in hydrophobic intersubunit interactions in the dimeric form (*10*, *11*, *21*). These interactions are determined to induce the dimeric state of the native protein (*10*, *11*, *21*). It is therefore reasonable that, once the hydrophobic interactions producing

the dimeric form are eliminated, this loop is dramatically affected. In the protein region of residues 50−59, we have not been able to assign five backbone HN signals out of ten amino acids. This could be due to an exchange broadening of these signals due to the large exposure of the corresponding protons to the solvent. Furthermore, in this region, several connectivities, which are expected on the basis of the structure, have not been identified due to the lack of NH signals. However, the backbone conformation of this region in all the available X-ray structures of SOD lies substantially inside the family.

Loop VI (residues 102−114) is also partially involved in intersubunit interactions in the dimeric protein. As it occurs for residues 50−68, the disorder observed for residues 107−110 can be reasonably ascribed to the absence of the second subunit in the monomer.

The overall picture is that, while loops I, III, and V are quite well-defined, even loops II, IV, and VI are much more disordered. This quite systematic behavior could be related to the fact that odd loops lie on the opposite side of the barrel with respect to the protein region involved in the formation of the dimer. The even loops constitute the most critical part of the protein as they either define the active site channel (loop IV) or define the interface between the monomeric units (loops IV and VI). Furthermore, on average, even loops are always longer than odd loops. This could be responsible for the larger mobility. It is therefore evident that, when the interactions that stabilize the dimeric form are eliminated, the regions of the subunits interacting with each other are now exposed to the solvent and may be less restricted in their internal motions, thus producing a loss of resolution in those regions. The extent and time scale of these motions are under investigation.

In addition to the extensive β-strand structure, a short α-helix is formed in the segment of residues 132−137. Such a helix is stabilized by the H-bond between the CO of Thr 135 and the peptide NH of the zinc-bound His 71. The latter is in turn H-bonded also to the carboxylic group of Asp 124 which forms H-bonds with both His 71 (zinc-bound) and His 46 (copper-bound). Such a network of H-bonds is conserved in all the X-ray structures of the dimeric isoenzymes and was previously proposed (*11*) to have an important role in stabilizing the active site structure and in determining the orientation of the α-helix with respect to the active cavity. As the α-helix contains several charged residues, its orientation is relevant for determining the electrostatic potential at the active site channel (*11*).

The presence of the Cys−Cys bond between residues 146 and 57, where the latter residue has been proposed to stabilize the orientation of Arg 143 (*11*), can be inferred from the chemical shift values of Cys 146 that are typical of a cystine residue (*59*). Furthermore, SDS−polyacrylamide gel electrophoresis clearly showed the presence of a cystine bridge in solution. As they are the only two Cys residues in this protein, Cys 146 and Cys 54 are bound by a disulfide bridge.

Relevant H-Bonds. Several authors pointed out, over the years, the relevance and the role of several H-bonds in the structures of the dimeric proteins that are largely conserved over most of the known isoenzymes (*10*, *11*, *71*). In particular, the occurrence of some H-bonds involving side chains of invariantly conserved residues with backbone atoms has been noted. Such interactions have been pointed out because of their role in "building" the Greek key structure and in "designing" the metal binding sites and the active cavity of the system. In this monomeric structure, the resolution of some side chains is such that some H-bonds are unambiguously identified. Therefore, it has been possible to observe a few differences in these interactions. In the dimeric form, Asn 86 is H-bonded to Gly 44 and Asp 124. These H-bonds are not observed in the present structure. Indeed, Asn 86 shows a completely different orientation of the χ_2 angle that prevents the formation of these two H-bonds. The H-bond between Arg 115 and Glu 49 is not observed in the present structure because of the high disorder of these residues. Arg 115 also makes H-bonds with Ser 111 in the dimeric proteins. The latter residue is well-resolved (and conserves all its H-bonds that are important for the thermal stability of the protein) in the present monomeric structure, but it is displaced with respect to the position in the dimeric enzyme. Although Arg 115 is quite disordered, it is likely that such a H-bond is effectively missing in the present derivative. The two residues are quite close to the subunit−subunit interface. The role of such a H-bond is to connect loop IV and loop VI, which form the "base" of the barrel. Again, this could be related to the monomerization of the protein.

Metal Sites. The copper ligands are well-defined with a single conformation. A stereoview of the structure of the active site is shown in Figure 5. For all residues but Asp 83, the rmsd values calculated by considering all heavy atoms are smaller than 1.0 Å, i.e., by far smaller than the average rmsd values observed for the other parts of the protein. The rmsd between the average position of the seven ligands of the metal ions of this monomeric structure and those of the reduced form of the dimeric yeast SOD is 0.44 Å. It is apparent that there are no major differences between the structure of the metal ligands of the dimeric protein and of the monomeric mutant, with the exception of the bridging histidine.

In the present structure, the copper(I) ion is tricoordinated, while the zinc is regularly tetracoordinated. The HN imidazole protons are solvent-exposed, consistent with their exchangeability with the bulk solvent. His 63 is protonated at the Nϵ2 position, the bound proton resonating at 12.6 ppm. His 63 is bound to zinc and points toward copper outside its coordination sphere. The distance between copper and Nϵ2 is now 3.5 Å, while it is 3.2 Å in yeast SOD (*20*). This distance, in the structure of the reduced dimeric bovine enzyme, is as short as 2.3 Å (*19*), consistent with the presence of the coordination bond between Cu and His 63. The distance between copper and the hydrogen Hϵ2 of His 63 is 3.0 Å in the present structure, which is consistent with the van der Waals distance, whereas the value of 2.6 Å, reported for reduced yeast SOD, violates the van der Waals distance. NMR provides unambiguous experimental evidence that His 63 is not coordinated to the copper ion. This is consistent with what was previously described for the dimeric protein, in the native state (*25*, *40*) and in the cobalt(II)-substituted derivative (*41*). Analogous coordination geometry for the copper ion was previously proposed from NMR data in the native, reduced form of the M2SOD monomeric adduct (*39*). In only one X-ray report on the reduced bovine enzyme, His 63 was found to be still bridging the two metal sites (*19*).

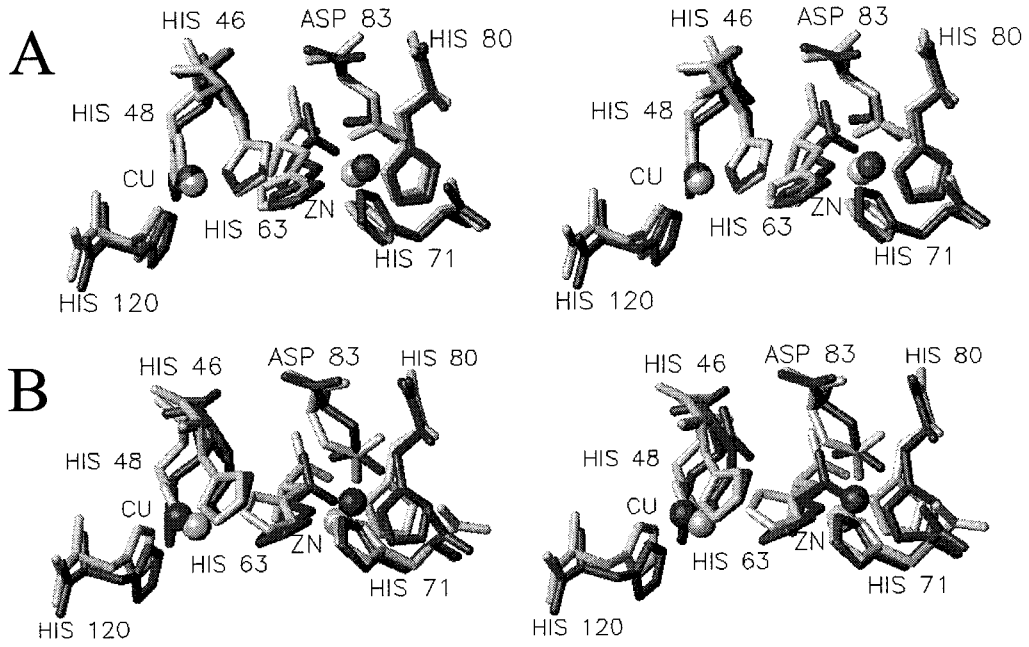

FIGURE 5: (A) Stereoview of the active sites of the reduced human monomer (Q133M2SOD) (black) (present structure) and of the reduced yeast dimer (gray) (*20*). (B) Stereoview of the active sites of the reduced human monomer (Q133M2SOD) (black) (present structure) and of the oxidized human dimer (gray) (*21*). The spheres represent the van der Waals radius of the metal ions.

While the position of metal ion ligands is very close to that in the reduced dimeric yeast isoenzyme, the copper ion experiences an average movement of about 0.6 Å away from His 63 and downward in the cavity. This movement is even larger with respect to the X-ray structure of the dimeric reduced bovine SOD (1.2 Å) where the bridge is intact (Figure 5). The position of copper in the latter protein is relatively close to that found in the oxidized form of the same bovine isoenzyme. Also, the zinc ion experiences a movement, in the opposite direction with respect to copper; thus, their distance is 7.2 Å in the present monomeric protein, while it is 6.7 Å in reduced yeast SOD. His 63 in the present structure follows the zinc ion in this movement, thus contributing to the increase in the distance between copper and His 63.

The movement is the opposite of that occurring during anion binding to copper(II). Such movement had been proposed on a spectroscopic basis (*72*) and later confirmed by X-ray studies (*73*).

Active Site Channel. The active site channel is formed by electrostatic loop VII which also contains the short α-helix, on one side, and by loop IV on the other. It has been previously proposed that a H-bonding network inside the cavity, formed by the side chains of some residues belonging to loop VII, plays a major role in increasing the diffusion rates of the superoxide radical inside the cavity (*31*). Such a network is supposed to optimize the conformation of the electrostatic loop for driving superoxide toward Arg 143 and stabilizing it (*26*, *35*, *74*). The interaction betweeen superoxide and Arg 143 is the last step for superoxide before the electron transfer occurs. Facing Arg 143 there is a Thr residue (Thr 137), which belongs to the electrostatic loop. Arg 143 and Thr 137 form a sort of bottleneck in the active cavity. The X-ray structures of various dimeric isoenzymes, both in the oxidized and in the reduced state, show no significant changes in the orientation of the side chains of Arg 143 and Thr 137. On the other hand, the side chains of the other residues belonging to the electrostatic loop, i.e., Glu 132, Glu 133, and Lys 136, are oriented differently in the various isoenzymes, whereas the oxidation state of copper does not seem to affect their position. Glu 133 is invariantly H-bonded to the hydroxyl group of Thr 137, and the Lys 136−Glu 132 and the Thr 137−Glu 133 H-bonds are well-conserved.

The active site channel of the present monomer, compared with the X-ray data of the oxidized dimeric protein from the same source (i.e., the human isoenzyme), is shown in Figure 6. In the present system, the Glu 133 is replaced by a Gln. The backbone and the side chain of Thr 137 remain almost unaltered with respect to the X-ray structure of the oxidized dimeric protein. However, in the present case, the oxygen and not the proton is involved in the H-bond with Gln 133. In other words, Thr 137 is transformed from proton donor to proton acceptor.

We observe that Glu 132 and Gln 133, which point toward the copper ion, have slightly shorter distances from the copper ion than they have in the human wild type oxidized protein. The side chain of Lys 136 is moved toward residue 133 and toward the internal surface of the cavity. The Nζ of Lys 136 is 11.5 Å from copper which should be compared with 13.2 Å in the human oxidized dimeric enzyme. Glu 132 moves in such a way that its negative COO^- carboxylate group is almost in the same place where the positive NH_3^+ of Lys 136 is in the dimeric protein. No H-bond is formed with either Gln 133 or Glu 132 (Figure 6).

The Thr 58, belonging to loop IV, that faces Glu 132 and Glu 133 and defines the "top" of the active cavity is 14.0 Å from the copper ion. Therefore, the shallow crevice of the active site channel is about 14 Å deep and 19 Å wide (the Thr 58 Cγ−Glu 132 Oϵ distance is 19 Å on average). The width of the shallow crevice is decreased by about 3 Å with respect to that of the human oxidized dimeric protein, where it is about 22 Å.

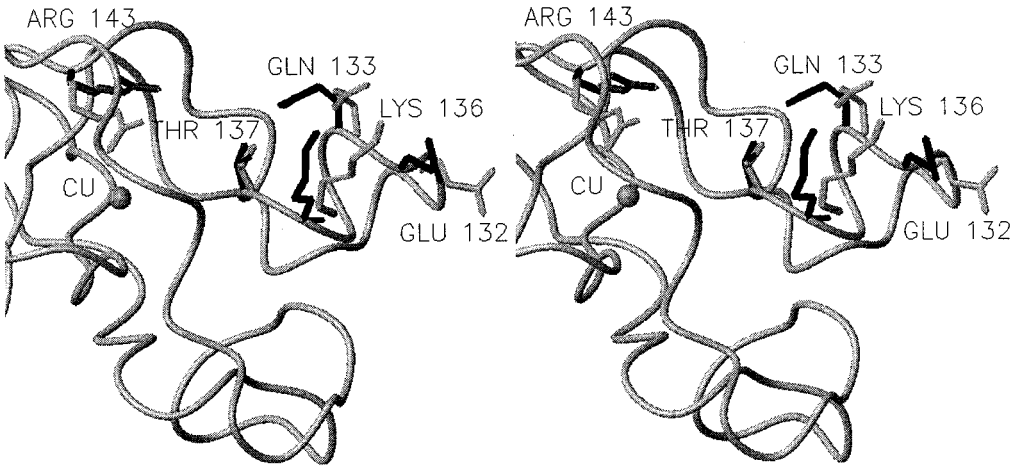

FIGURE 6: Stereoview of the active site channel of the reduced human monomer (Q133M2SOD) (black) (present structure) and of the oxidized human dimer (gray) (*21*).

Although both loops IV and VII are relatively disordered, the residues forming the active site cavity are well-defined. The side chain of Arg 143, belonging to loop VII, is tilted up with respect to its original position in the human oxidized dimeric enzyme. The position of Arg 143 in the latter is determined by the three H-bonds occurring between the carbonyl oxygens of Cys 57 and Gly 61 and protons of both Nη1 and Nη2 groups of Arg 143 and between the carbonyl oxygen of Thr 58 and one Nη2 proton of Arg 143. None of these H-bonds is observed in the present structure. This is due to the disorder of Cys 57 and Thr 58. Indeed, they are in the most disordered region of loop IV. This disorder leads to the breaking of the H-bonds with the guanidinium group of Arg 143. The consequence is that the latter moves away from its position (3 Å, on average), and is less buried in the cavity. The Cu−Nη1 and −Nη2 (Arg 143) distances are increased by about 2 Å; they are 8.0 and 8.6 Å in the monomer and 5.6 and 7.1 Å in the dimer. This increase in distance is due to the movement of Arg 143, which is partially balanced by the movement of copper (see Figure 6).

As the electrostatic field produced by the active channel is of great relevance for attracting superoxide to the active site and therefore for determining the catalytic rates, an analysis of the changes in this field determined by the structural changes is quite significant. In Figure 7, the electrostatic potential surfaces of the present structure and of a reduced and oxidized form are shown. The present reduced monomeric form is characterized by a relatively small surface with a positive potential, just at the bottom of the active channel, which is surrounded by large areas of protein with negative electrostatic potentials. On the contrary, the reduced form of a subunit of yeast SOD, which is characterized by the same charges at the copper site, shows a more extensive positive surface. Also, a single subunit of the human oxidized SOD, which has the same charge as the reduced form with the broken bridge, has a larger positive surface around the entrance of the active site channel. The comparison of the distribution of the electrostatic potential on the surface of the single subunit and of the entire dimer of the oxidized human structure indicates that the increased positive potentials on the rims and in the active channel are not affected by the presence of the other subunit, thus being essentially determined by the conformation of the charged residues in electrostatic loop VII.

Implications for the Mechanisms. The present solution structure of a monomeric form of SOD can shed light on a few aspects of the enzymatic mechanism of SOD and on the factors affecting the catalytic rates. In this reduced monomeric form, the bridge between copper and zinc is invariantly found to be broken in solution, as in the case of all the other investigated reduced isoenzymes.

Upon reduction, a hydrogen atom is needed to protonate His 63. The position of this proton is at van der Waals distance from copper(I) and is strategically located to be involved in the catalytic mechanism, presumably by interacting with O_2^- (*22*). A H-bond between His 63 and O_2^- could be the responsible for the attraction of an electron from copper(I) to O_2^-, with the subsequent formation of HO_2^-.

The coordination properties of copper are only sligthly affected by the monomerization which, however, induces a reduction in the catalytic rates of about one order of magnitude. It had been previously proposed that the geometry of copper has little influence on the catalytic rates (*28*). Furthermore, the reduction potential of the copper ion, even if slightly lowered[1], is still suitable for performing O_2^- dismutation as the monomeric form still performs the two reactions, even if at lower rates. On the contrary, point mutations of residues in the active site channel do affect such rates (*28*, *29*, *33*). Indeed, the conformation of the side chains of residues belonging to the electrostatic loop, important for determining the catalytic rates, is strongly affected by monomerization. The conformations in this loop are substantially independent of the oxidation state, as observed by comparing the oxidized and reduced X-ray structures of the bovine and yeast isoenzymes and as it would be inferred from the identity of the catalytic rates for the oxidized and reduced forms of the enzyme (*6*, *75*). Relevant for the efficiency of the catalytic function may be the change in position of the positive guanidinium group of Arg 143, which in the present system is further from the copper ion and therefore from the reaction site.

[1] It has been spectrophotometrically observed that ferrocyanide is not able to reduce the copper(II) ion in this monomeric form, which is however reduced by ascorbate.

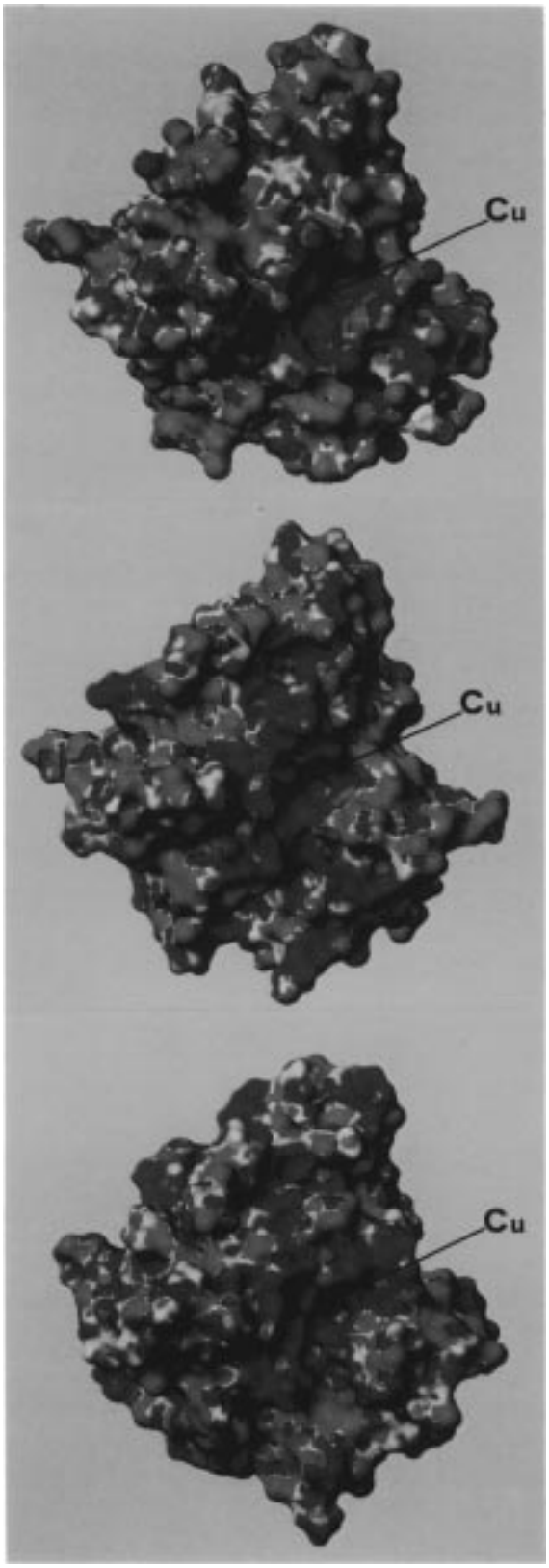

FIGURE 7: Electrostatic potential mapped onto the surface of the reduced human monomer (Q133M2SOD) (top), reduced yeast dimer (middle), and oxidized human dimer (bottom). The electrostatic potential is color-coded with red for negatively charged, blue for positively charged, and gray for neutral regions. The position of the copper ion is indicated. The figure was drawn with MOLMOL (*78*).

In the present monomeric structure, despite Glu 133 being neutralized, the electrostatic field at the entrance of the channel is much less positive than in all the dimeric forms for which the structure is available. Therefore, the conformations of loop VII and of Arg 143 in the monomeric form of SOD are not optimized for fast diffusion rates of the substrate at the reaction site.

CONCLUDING REMARKS

SOD is an important metalloenzyme both for its biological role in oxygen and radical scavenging and for its possible use in organ preservation. The presence of SOD mutants has been tentatively related to familial amyotrophic lateral sclerosis (FALS) pathology (*21*, *76*, *77*). The solution structure of the reduced state of a monomeric form, here determined for the first time, has shown that the folding is the same for all the known SOD structures, with the typical eight-stranded β-barrel. At the metal sites, the structure is similar, though not identical, to one of the two crystal structures of the reduced state (*20*), with the imidazolate bridge between copper and zinc clearly broken at the copper site. The charged residues, which form and surround the active site channel, have quite different conformations with respect to dimeric proteins which produce a less positive electrostatic potential at the entrance of the channel. It turns out that the electrostatic potential and size of the active site channel are optimized for O_2^- diffusion in the wild type dimeric protein. In the present monomeric species, where the activity is about one order of magnitude smaller, the orientation of several residues, e.g., Arg 143, etc., is different from that in the WT dimeric protein. This is, at least partly, due to the absence of a second subunit which is capable of ordering the active channel and of providing a favorable orientation of the residues inside the active site channel, thus affecting the electrostatic potential.

The correct location of Hδ2 of His 63 which is close, at van der Waals distance from copper(I), is an important structural result. This proton maintains the same charge at the active site, both in the oxidized and in the reduced proteins. Its location is presumably relevant for attracting one electron from copper to superoxide and for the formation of H_2O_2.

ACKNOWLEDGMENT

Thanks are expressed to Prof. Stefano Mangani for helpful discussion and to Dr. Antonio Rosato and Dr. Paolo Carloni for their assistance in performing relaxation matrix calculations and electrostatic potential calculations, respectively. We are also grateful to Dr. Thierry Richert and to Dr. Roberto Fadin for their contribution. The SON NMR LSF Utrecht, directed by Professor R. Kaptein, and the Frankfurt LSF, directed by Professor H. Rüterjans, are acknowledged for allowing us to perform some heteronuclear experiments.

SUPPORTING INFORMATION AVAILABLE

A table listing the ^1H, ^{13}C, and ^{15}N resonance assignments of reduced monomeric Q133M2 Cu,ZnSOD at 298 K and pH 5.0 (4 pages). Ordering information is given on any current masthead page.

REFERENCES

1. Fridovich, I. (1986) *Adv. Enzymol. Relat. Areas Mol. Biol. 58*, 61−97.

2. Valentine, J. S., and Pantoliano, M. W. (1981) in *Metal Ions in Biological Systems* (Sigel, H., Ed.) Vol. 3, pp 291−358, Dekker, New York.
3. Bertini, I., Mangani, S., and Viezzoli, M. S. (1998) in *Advanced Inorganic Chemistry* (Sykes, A. G., Ed.) pp 127−250, Academic Press, San Diego.
4. McCord, J. M., and Fridovich, I. (1969) *J. Biol. Chem. 244*, 6049−6055.
5. Fee, J. A., and Gaber, B. P. (1972) *J. Biol. Chem. 247*, 60.
6. Klug, D., Rabani, J., and Fridovich, I. (1972) *J. Biol. Chem. 247*, 4839−4842.
7. Cabelli, D. E., and Bielski, B. H. (1983) *J. Phys. Chem. 87*, 1809−1812.
8. Bull, C., and Fee, J. A. (1985) *J. Am. Chem. Soc. 107*, 3295−3304.
9. Fee, J. A., and Bull, C. (1986) *J. Biol. Chem. 261*, 13000−13005.
10. Tainer, J. A., Getzoff, E. D., Beem, K. M., Richardson, J. S., and Richardson, D. C. (1982) *J. Mol. Biol. 160*, 181−217.
11. Parge, H. E., Hallewell, R. A., and Tainer, J. (1992) *Proc. Natl. Acad. Sci. U.S.A. 89*, 6109−6114.
12. Desideri, A., Falconi, M., Polticelli, F., Bolognesi, M., Djinovic, K., and Rotilio, G. (1992) *J. Mol. Biol. 223*, 337−342.
13. Kitagawa, Y., Tanaka, N., Hata, Y., Kusonoki, M., Lee, G., Katsube, Y., Asada, K., Alibara, S., and Morita, Y. (1991) *J. Biochem. 109*, 447−485.
14. Djinovic, K., Gatti, G., Coda, A., Antolini, L., Pelosi, G., Desideri, A., Falconi, M., Marmocchi, F., Rotilio, G., and Bolognesi, M. (1992) *J. Mol. Biol. 225*, 791−809.
15. Djinovic, K., Coda, A., Antolini, L., Pelosi, G., Desideri, A., Falconi, M., Rotilio, G., and Bolognesi, M. (1992) *J. Mol. Biol. 226*, 227−238.
16. Djinovic, C., Battistoni, A., Carrì, M., Polticelli, F., Desideri, A., Rotilio, G., Coda, A., Wilson, K., and Bolognesi, M. (1996) *Acta Crystallogr. D52*, 176−188.
17. McRee, D. E., Redford, S. M., Getzoff, E. D., Lepock, J. R., Hallewell, R. A., and Tainer, J. A. (1990) *J. Biol. Chem. 265*, 14234−14241.
18. Roberts, V. A., Fisher, C. L., Redford, S. M., McRee, D. E., Parge, H. E., Getzoff, E. D., and Tainer, J. A. (1990) *Free Radical Res. Commun. 12−13*, 269−278.
19. Banci, L., Bertini, I., Bruni, B., Carloni, P., Luchinat, C., Mangani, S., Orioli, P. L., Piccioli, M., Rypniewski, W., and Wilson, K. (1994) *Biochem. Biophys. Res. Commun. 202*, 1088−1095.
20. Ogihara, N. L., Parge, H. E., Hart, J. P., Weiss, M. S., Goto, J. J., Crane, B. R., Tsang, J., Slater, K., Roe, J. A., Valentine, J. S., Eisenberg, D., and Tainer, J. A. (1996) *Biochemistry 35*, 2316−2321.
21. Deng, H.-X., Hentati, A., Tainer, J. A., Lqbal, Z., Cyabyab, A., Hang, W.-Y., Getzoff, E. D., Hu, P., Herzfeldt, B., Roos, R. P., Warner, C., Deng, G., Soriano, E., Smyth, C., Parge, H. E., Ahmed, A., Roses, A. D., Hallewell, R. A., Pericak-Vance, M. A., and Siddique, T. (1993) *Science 261*, 1047−1051.
22. Tainer, J. A., Getzoff, E. D., Richardson, J. S., and Richardson, D. C. (1983) *Nature 306*, 284−287.
23. Blackburn, N. J., Hasnain, S. S., Binsted, N., Diakun, G. P., Garner, C. D., and Knowles, P. F. (1984) *Biochem. J. 219*, 985−990.
24. Bertini, I., Banci, L., Brown, R. D., III, Koenig, S. H., and Luchinat, C. (1988) *Inorg. Chem. 27*, 951−953.
25. Murphy, L. M., Strange, R. W., and Hasnain, S. (1997) *Structure 5*, 371−379.
26. Beyer, W. F., Jr., Fridovich, I., Mullenbach, G. T., and Hallewell, R. A. (1987) *J. Biol. Chem. 262*, 11182−11187.
27. Bertini, I., Banci, L., Luchinat, C., and Hallewell, R. A. (1988) in *Annals of the New York Academy of Sciences* (Blanch, H. W., and Klibanov, A. M., Eds.) pp 37−52, New York Academy of Science Books, New York.
28. Bertini, I., Banci, L., Luchinat, C., Bielski, B. H. J., Cabelli, D., Mullenbach, G. T., and Hallewell, R. A. (1989) *J. Am. Chem. Soc. 111*, 714−719.
29. Banci, L., Bertini, I., Cabelli, D., Hallewell, R. A., Luchinat, C., and Viezzoli, M. S. (1990) *Inorg. Chem. 29*, 2398−2403.
30. Banci, L., Bertini, I., Cabelli, D. E., Hallewell, R. A., Luchinat, C., and Viezzoli, M. S. (1991) *Free Radical Res. Commun. 12−13*, 239−251.
31. Getzoff, E. D., Cabelli, D. E., Fisher, C. L., Parge, H. E., Viezzoli, M. S., Banci, L., and Hallewell, R. A. (1992) *Nature 358*, 347−351.
32. Banci, L., Bertini, I., Bauer, D., Hallewell, R. A., and Viezzoli, M. S. (1993) *Biochemistry 32*, 4384−4388.
33. Banci, L., Bertini, I., Luchinat, C., and Viezzoli, M. S. (1993) *Inorg. Chem. 32*, 1403−1406.
34. Banci, L., Cabelli, D. E., Getzoff, E. D., Hallewell, R. A., and Viezzoli, M. S. (1993) *J. Inorg. Biochem. 50*, 89−100.
35. Fisher, C. L., Cabelli, D. E., Tainer, J. A., Hallewell, R. A., and Getzoff, E. D. (1994) *Proteins: Struct., Funct., Genet. 19*, 24−34.
36. Polticelli, F., Battistoni, A., Bottaro, G., Carri, M. T., O'Neill, P., Desideri, A., and Rotilio, G. (1994) *FEBS Lett. 352*, 76−78.
37. Polticelli, F., Battistoni, A., O'Neill, P., Rotilio, G., and Desideri, A. (1996) *Protein Sci. 5*, 248−253.
38. Malinowski, D., and Fridovich, I. (1979) *Biochemistry 18*, 237−244.
39. Bertini, I., Piccioli, M., Viezzoli, M. S., Chiu, C. Y., and Mullenbach, G. T. (1994) *Eur. J. Biophys. 23*, 167−176.
40. Bertini, I., Capozzi, F., Luchinat, C., Piccioli, M., and Viezzoli, M. S. (1991) *Eur. J. Biochem. 197*, 691−697.
41. Bertini, I., Luchinat, C., and Monnanni, R. (1985) *J. Am. Chem. Soc. 107*, 2178−2179.
42. Banci, L., Bertini, I., Chiu, C. Y., Mullenbach, G. T., and Viezzoli, M. S. (1995) *Eur. J. Biochem. 234*, 855−860.
43. Banci, L., Benedetto, M., Bertini, I., Del Conte, R., Piccioli, M., Richert, T., and Viezzoli, M. S. (1998) *Magn. Reson. Chem. 35*, 845−853.
44. Logan, T. M., Olejniczak, E. T., Xu, R. X., and Fesik, S. W. (1993) *J. Biomol. NMR 3*, 225.
45. Kay, L. E., Xu, G., Singer, A. U., Muhandiram, D. R., and Forman-Kay, J. D. (1993) *J. Magn. Reson., Ser. B 101*, 333−337.
46. Wider, G., Neri, D., Otting, G., and Wüthrich, K. (1989) *J. Magn. Reson. 85*, 426−431.
47. Vuister, G. W., and Bax, A. (1993) *J. Am. Chem. Soc. 115*, 7772−7777.
48. Marion, D., and Wüthrich, K. (1983) *Biochem. Biophys. Res. Commun. 113*, 967−974.
49. Piotto, M., Saudek, V., and Sklenar, V. (1992) *J. Biomol. NMR 2*, 661−666.
50. States, D. J., Habenkorn, R. A., and Ruben, D. J. (1982) *J. Magn. Reson. 48*, 286−292.
51. Eijkelenboom, A. P., van den Ent, F. M., Vos, A., Doreleijers, J. F., Hard, K., Tullius, T. D., Plasterk, R. H., Kaptein, R., and Boelens, R. (1997) *Curr. Biol. 7*, 739−746.
52. Güntert, P., Dotsch, V., Wider, G., and Wüthrich, K. (1992) *J. Biomol. NMR 2*, 619−629.
53. Eccles, C., Güntert, P., Billeter, M., and Wüthrich, K. (1991) *J. Biomol. NMR 1*, 111−130.
54. Güntert, P., Braun, W., and Wüthrich, K. (1991) *J. Mol. Biol. 217*, 517−530.
55. Weisemann, R., Rüterjans, H., Schwalbe, H., Schleucher, J., Bermel, W., and Griesinger, C. (1994) *J. Biomol. NMR 4*, 231−240.
56. Bax, A., and Wang, A. C. (1995) *J. Am. Chem. Soc. 117*, 1810−1813.
57. Karimi-Nejad, Y., Schmidt, J. M., and Rüterjans, H. (1994) *Biochemistry 33*, 5481−5492.
58. Güntert, P. (1995) in *DIANA Program version 2.8 User Manual and Instructions*, Insitut für Molekularbiologie und Biophysik Eidgenössische Technische Hochschule-Höngger-berg, Zürich, Switzerland.
59. Wishart, D. S., Sykes, B. D., and Richards, F. M. (1991) *J. Mol. Biol. 222*, 311−333.

60. Pearlman, D. A., Case, D. A., Caldwell, G. C., Siebel, G. L., Singh, U. C., Weiner, P., and Kollman, P. A. (1991) in *AMBER 4.0*, University of California, San Francisco.
61. Banci, L., Carloni, P., and Orioli, P. L. (1994) *Proteins: Struct., Funct., Genet. 18*, 216−230.
62. Banci, L., Bertini, I., Eltis, L. D., Felli, I. C., Kastrau, D. H. W., Luchinat, C., Piccioli, M., Pierattelli, R., and Smith, M. (1994) *Eur. J. Biochem. 225*, 715−725.
63. Laskowski, R. A., Rullmann, J. A. C., MacArthur, M. W., Kaptein, R., and Thornton, J. M. (1996) *J. Biomol. NMR 8*, 477−486.
64. Hore, P. J. (1983) *J. Magn. Reson. 54*, 539−542.
65. Van Dijk, A. A., Scheek, R. M., Dijkstra, K., Wolters, G. K., and Robillard, G. T. (1992) *Biochemistry 31*, 9063−9072.
66. Blomberg, F., Maurer, W., and Ruterjans, H. H. (1977) *J. Am. Chem. Soc. 99*, 8149−8159.
67. Chen, Y.-L., Park, S., Thornburg, R. W., Tabatabai, L. B., and Kintanar, A. (1995) *Biochemistry 34*, 12265−12275.
68. Bertini, I., Donaire, A., Feinberg, B. A., Luchinat, C., Piccioli, M., and Yuan, H. (1995) *Eur. J. Biochem. 232*, 192−205.
69. James, T. L., Borgias, B., Bianucci, A. M., and Zhou, N. (1991) in *NMR and Biomolecular Structure* (Bertini, I., Molinari, H., and Niccolai, N., Eds.) pp 87−111, VCH, Weinheim, Germany.
70. Borgias, B., Thomas, P. D., and James, T. L. (1989) in *Complete Relaxation Matrix Analysis (CORMA)*, University of California, San Francisco.
71. Bordo, D., Djinovic, K., and Bolognesi, M. (1994) *J. Mol. Biol. 238*, 366−386.
72. Banci, L., Bencini, A., Bertini, I., Luchinat, C., and Piccioli, M. (1990) *Inorg. Chem. 29*, 4867−4873.
73. Djinovic, K., Polticelli, F., Desideri, A., Rotilio, G., Wilson, K., and Bolognesi, M. (1994) *J. Mol. Biol. 240*, 179−183.
74. Banci, L., Bertini, I., Luchinat, C., and Hallewell, R. A. (1988) *J. Am. Chem. Soc. 110*, 3629−3633.
75. Bray, R. C., Clocke, S. A., Fielden, E. M., Roberts, P. B., Rotilio, G., and Calabrese, L. (1974) *Biochem. J. 139*, 43−48.
76. Rosen, D. R., Siddique, T., Patterson, D., Figlewicz, D. A., Sapp, P., Hentati, A., Donaldson, D., Goto, J., O'Regan, J., Deng, H.-X., Rahmani, Z., Krizus, A., McKenna-Yasek, D., Cayabyab, A., Gatson, S. M., Berger, R., Tanzi, R. E., Halperin, J. J., Herzfeldt, B., van der Bergh, R., Hung, W.-Y., Deng, G., Mulder, D. W., Smyth, C., Laing, N. G., Soriano, E., Pericak-Vance, M. A., Haines, J., Rouleau, G. A., Gusella, J. S., Horvitz, H. R., and Brown, R. H., Jr. (1993) *Nature 362*, 59−62.
77. Wiedau-Pazos, M., Goto, J. J., Rabizadeh, S., Gralla, E. B., Roe, J. A., Lee, M. K., Valentine, J. S., and Bredesen, D. E. (1996) *Science 271*, 515−518.
78. Koradi, R., Billeter, M., and Wüthrich, K. (1996) *J. Mol. Graphics 14*, 51−55.

BI9803473